The Drift Flux Model in the ASSERT Subchannel Code

M.B. Carver, R.A. Judd, J.C. Kiteley, and A. Tahir
Thermalhydraulics Development Branch
Atomic Energy of Canada Limited
Chalk River Nuclear Laboratories
Chalk River, Ontario

Abstract
The ASSERT subchannel code has been developed specifically to model flow and phase distributions within CANDU fuel bundles. ASSERT uses a drift-flux model that permits the phases to have unequal velocities, and can thus model phase separation tendencies that may occur in horizontal flow. The basic principles of ASSERT are outlined, and computed results are compared against data from various experiments for validation purposes. The paper concludes with an example of the use of the code to predict critical heat flux in CANDU geometries.

Résumé
Le logiciel de sous-canaux ASSERT a été développé dans le but de modéliser l'écoulement diphasique du caloporteur dans les grappes de combustible nucléaire du type CANDU. Basé sur un modèle à écart de vitesses, ASSERT permet de prédire les vitesses inégales des phases et par conséquent de modéliser leur séparation dans un écoulement horizontal. On discute brievement le modèle physique d'ASSERT et les résultats numériques sont comparés aux résultats expérimentaux. On conclue avec un exemple d'application d'ASSERT pour la prédiction du flux de chaleur critique dans un canal de réacteur CANDU.

Introduction

As a nuclear reactor system relies entirely on fluid circuits for energy transport, mathematical modelling of thermalhydraulic phenomena plays an important role in reactor design and development, and methods of improving the accuracy and efficiency of thermal-hydraulic computations are sought continually. In a CANDU reactor for example, the fluid behaviour may be adequately described by one-dimensional (cross-sectional averaged) models throughout most of the piping network. However, in the reactor fuel channel, flow must distribute itself amongst the intricate flow passages of the fuel bundle. One-dimensional analysis is adequate here to simulate overall or bulk energy transfer, but multi-dimensional analysis is necessary to model detailed local distribution of flows and temperatures inside this complex geometry. In particular, the conventional method of predicting critical heat flux (CHF) for natural-uranium-fuelled CANDU bundles is by applying a CHF correlation based on one-dimensional (cross-sectional-averaged) flow parameters. Such correlations are derived from curve fits to CHF data measured in experiments designed to simulate closely the geometry and heat flux distribution in CANDU bundles. These correlations are adequate to predict behaviour of current reactors, but would not be applicable to any future designs that have radical changes in radial flux distribution or geometry, as such changes may significantly alter the distribution of flow within the fuel bundle. These variations can be assessed only by another experiment, or by introducing a multi-dimensional flow calculation, for example in a subchannel code. In such a code, local flow and void distributions are calculated within the individual 'subchannels' or passages between fuel rods, and a local CHF correlation is then applied to each subchannel to assess when these local conditions will generate CHF.

The ASSERT subchannel code [1] has been developed to address the computation of flow and phase distribution within the subchannels of CANDU bundles, which are horizontal. Unlike conventional subchannel codes such as COBRA [2], which are designed primarily to model flow in vertical fuel bundles, and use a homogeneous mixture model of two-phase flow, ASSERT uses a drift-flux model that permits the phases to have unequal velocities, and includes gravity terms that make it possible to analyze separation tendencies that may occur in horizontal flow.

The development of ASSERT has included validation by comparison of computed results to data from a number of experiments involving two-phase flow in horizontal channels [3] and vertical bundles [4, 5]. Recently, ASSERT predictions of CHF have also been compared to the U1 horizontal 37-rod bundle experiments.

Keywords: subchannel, drift-flux, two-fluid, two-phase, critical heat flux, void fraction, separation.

Thermalhydraulic Model

The thermalhydraulic model equations used in ASSERT-4 (Version 1) are derived from the two-fluid formulation. The two-fluid equations are combined to obtain the ASSERT model equations. The transportive form is obtained from the conservative form merely by subtracting the identity expressed by the mass equations. ASSERT has options to solve either of the two-fluid equations, using either the drift-flux or the homogeneous mixture model.

Conservation Equations

Mixture mass (conservative form) is

$$\frac{\partial \rho}{\partial t} + \nabla \cdot (\rho V) = 0 \tag{1}$$

where

$$\rho = (\alpha \rho)_g + (\alpha \rho)_f = \alpha_g^+ \rho_g + \alpha_f^+ \rho_f$$
$$(\rho V) = (\alpha \rho V)_g + (\alpha \rho V)_f = \rho V.$$

Mixture momentum (conservative form) is

$$\frac{\partial (\rho V)}{\partial t} + \nabla \cdot \left(\rho VV + \frac{(\alpha \rho)_g (\alpha \rho)_f}{\rho} V_r V_r^+ \right) + \nabla P = -F_w^+ + \rho g. \tag{2}$$

Mixture energy (transportive form) is

$$\rho \frac{\partial h}{\partial t} + \rho V \cdot \nabla h + \nabla \cdot \left(\frac{(\alpha \rho)_g (\alpha \rho)_f}{\rho} (h_g - h_f) V_r^+ \right) =$$
$$q_w'''^+ - \nabla \cdot ((\alpha q'')_g + (\alpha q'')_f)^+. \tag{3}$$

Phasic energy (transportive form) liquid is

$$(\alpha \rho)_f \frac{\partial h_f}{\partial t} + (\alpha \rho V)_f \cdot \nabla h_f = q_{wf}'''^+ - \nabla \cdot (\alpha q'')_f^+ + q_{if}'''^+. \tag{4}$$

Phasic energy (transportative form) vapour is

$$(\alpha \rho)_g \frac{\partial h_g}{\partial t} + (\alpha \rho V)_g \cdot \nabla h_g = q_{wg}'''^+ - \nabla \cdot (\alpha q'')_g^+ + q_{ig}'''^+ \tag{5}$$

where

$$\alpha_g + \alpha_f = 1.$$

Henceforth, for simplicity we will use α to denote α_g.

+ – denotes variables that must be defined by state relationships; and

† – denotes variables that must be defined by constitutive relationships.

Subchannel Equations

ASSERT uses the subchannel approach used in the development of the COBRA-IV computer code [2]. Subchannels are defined as the flow areas between rods, bounded by the rods themselves and imaginary lines linking adjacent rod centres. Subchannels are divided axially into a number of control volumes that communicate axially with neighbours in the same subchannel and laterally across fictitious boundaries (gaps) with control volumes in neighbouring subchannels. The relationship between the reactor core, a fuel channel,
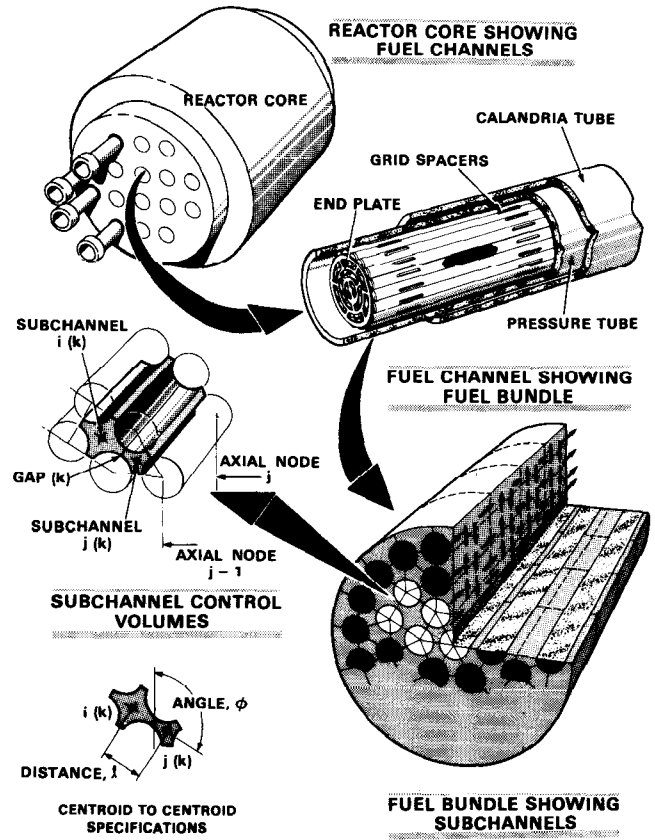

Figure 1: Formulation of subchannel control volume.

and the definition of particular subchannels is given in Figure 1.

The development of finite difference analogs to express the equations (1–5) with respect to subchannel control volumes follows the approach used in COBRA, but unlike COBRA, the transverse gravity terms are retained, making it possible to use ASSERT-4 to model the effect of gravity on horizontal two-phase flows even if the homogeneous option is used. Spatial-differenced versions of the model equations are derived by applying the conservation equations to a representative control volume taken from subchannel i(k) which shares gap k with an adjacent control volume in subchannel j(k) between axial nodes j-1 and j. Details are given in the user's manual [1].

Closure Relationships

The required closure relationships, as indicated above, are the equations of state and constitutive relationships relating relative velocity, fluid friction, wall heat transfer, and thermal mixing to primary variables, phasic flow velocities, densities, enthalpies, and pressure.

The relative velocity is the heart of the successful application of the ASSERT model to horizontal bundles and channels. It comprises several effects, including

1. relative velocity due to cross-section averaging;
2. local relative velocity due to gravity separation;

3. turbulent diffusion of void, both between neighbouring channels and towards a preferred phase distribution pattern.

The vapour phase velocity V_g is therefore considered to depart from the mixture volumetric flux, j, due to these effects, which are incorporated using, respectively, the Zuber-Findlay distribution parameter C_0, and the weighted mean velocity V_{gj} [6] and the void diffusion term [7].

$$V_g = C_0 j + V_{gj} - \frac{\varepsilon}{l\bar{\alpha}} \Delta_{ij}(\bar{\alpha} - \alpha_0) \qquad (6)$$

Noting that

$$j = \bar{\alpha} V_g + (1 - \bar{\alpha})V_f \qquad (7)$$

and

$$V_r = V_g - V_f$$

yields the expression for relative velocity required in equation 2.

$$V_r = \left[(C_0 - 1)j + V_{gj} - \frac{\varepsilon}{\bar{\alpha}l} \Delta_{ij}(\bar{\alpha} - \alpha_0) \right] / (1 - \bar{\alpha}) \qquad (8)$$

In the axial momentum equation only the first two terms in (8) are considered important. However, in the lateral momentum equation, according to the usual practice in subchannel analysis, void diffusion is considered dominant, and only the last two terms are used, as C_0 is also taken as unity.

$$U_r = \{(C_0 - 1)j + u_{gj}\}/(1 - \bar{\alpha}) \text{ (axial relative velocity)} \qquad (9)$$

$$V_r = \{(v_{gj} - (\varepsilon/\bar{\alpha}l)\Delta_{ij}(\bar{\alpha} - \alpha_0)\}/(1 - \bar{\alpha}) \text{ (lateral relative velocity)} \qquad (10)$$

The drift velocity of the bubbles, u_{gj}, is expressed in terms of terminal bubble rise velocity, V_∞, as follows:

$$V_{gj} = (1 - \bar{\alpha})^n V_\infty \cos \phi, \qquad (11)$$

where n may vary from zero to 3. V_∞ is the terminal bubble rise velocity, which can be expressed as

$$V_\infty = k_1 \left[\frac{(\rho_f - \rho_g)}{\rho_f^2} \sigma g \right]^{k_2} \qquad (12)$$

where ϕ is the direction angle of the connection between subchannels. This term models the gravity separation of the phases for horizontal flow.

The void diffusion term includes two effects: the turbulent diffusion of void fraction and the diffusion toward a nonuniform void. The parameter α_0 is an equilibrium void fraction included to account for the experimentally observed tendency of void to migrate toward larger subchannels, and is defined following Lahey [7]. The diffusion equation is expressed, as in the case of single-phase, in terms of the Peclet number ε_α / VD, from the work reported by Rudzinski [8] for void ranging between 0.30 and 0.6.

$$\varepsilon_\alpha / VD = C_\alpha (\alpha / 0.6)^6, \quad C_\alpha = 0.075 \qquad (13)$$

The equations 9–12 have a number of free parameters, for which constant values were used in earlier work

with ASSERT [3]. Recently, however, relationships proposed by Ohkawa and Lahey [9] have been incorporated. These give compatible definitions of u_{gj} and C_0 in terms of characteristic properties of two-phase flow. The parameters n, k_1, k_2, and C_0 are thus varied, appropriately, with void fraction and the ratio of phase densities, thus extending the applicable range of the drift-flux model. These relationships produced satisfactory results over a range of conditions except at high void fractions. It is clear from equation 8 that the relative velocity will become infinite as α approaches unity, and in fact when the Ohkawa-Lahey relationships are used to define C_0 and u_{gj}, equation 8 became indeterminate (0 / 0). A smoothing factor compatible with the Ohkawa-Lahey equations was introduced to ensure correct asymptotic behaviour. The resulting equations are summarized in Reference 1.

Solution Procedure
The numerical solution over the bundle cross-section at each axial position is split into two parts. The first part solves the energy and state equations, using a block iterative method to calculate the mixture and phasic enthalpies for all subchannels, where current flow estimates are used as parameters. Once the energy equation solution inner iteration converges, the second part calculates the flows and pressure gradients at that axial position. This is done by the direct matrix solution of the crossflow equations, from which it is possible to calculate axial flows and pressure gradients. Both parts are repeated once to ensure a higher level of convergence of both energy and flow solutions prior to moving to the next axial position. The channel is successively swept from the inlet to the exit. This outer iteration continues until convergence is achieved, or until an iteration limit is reached. Successful completion would yield a steady-state solution, or one time-step of a transient solution.

The ASSERT code can be run with either flow, or header-to-header pressure drop specified, and has been written in a plane-by-plane solution mode that eliminates any restriction on the number of axial nodes used.

CHF Methodology in ASSERT
The probability of making a successful prediction of local CHF obviously is a direct function of the success of predicting local flow and phase distribution. In ASSERT, the CHF prediction is performed subsequent to calculation of flow distribution.

Whalley et al. [10] developed a film boiling model to calculate CHF for vertical annular upflow in round tubes. The method is based on the assumption that the flow regime is annular. The essential features of annular flow are that the gas travels in the centre of the channel, a liquid film travels on the channel walls, and liquid drops are carried along with the gas flow. The

continuity equation for the film flow in the liquid annulus is written in terms of evaporation, entrainment, and deposition, and solved for the dryout point, at which film thickness is effectively zero. In ASSERT the equation is solved for each subchannel to predict the rod, subchannel, and axial location where dry-out occurs.

Validation Studies

The early part of ASSERT development concentrated on the development of a suitable thermalhydraulic model [3] and then on validation, which, of course, involves continuous development.

Comparison with Air / Water Twin Channel Experiments

The work of Tapucu on exchange of air-water mixtures flowing in two parallel square communicating channels was used for initial testing of the ASSERT code.
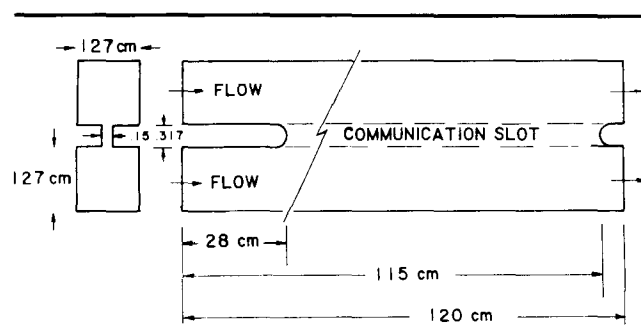

Figure 2: Geometry of the Tapucu experiment square subchannels.

Details of these experiments and the experimental technique are reported in reference [11]. Channel dimensions are given in Figure 2. The experiments were run at the same initial nominal mass flux of $3{,}060\,\mathrm{kg\,m^{-2}\,s^{-1}}$ in both subchannels, but for different initial voids and different orientations. The key parameters – pressure, void fractions, and liquid and gas flow rates in both
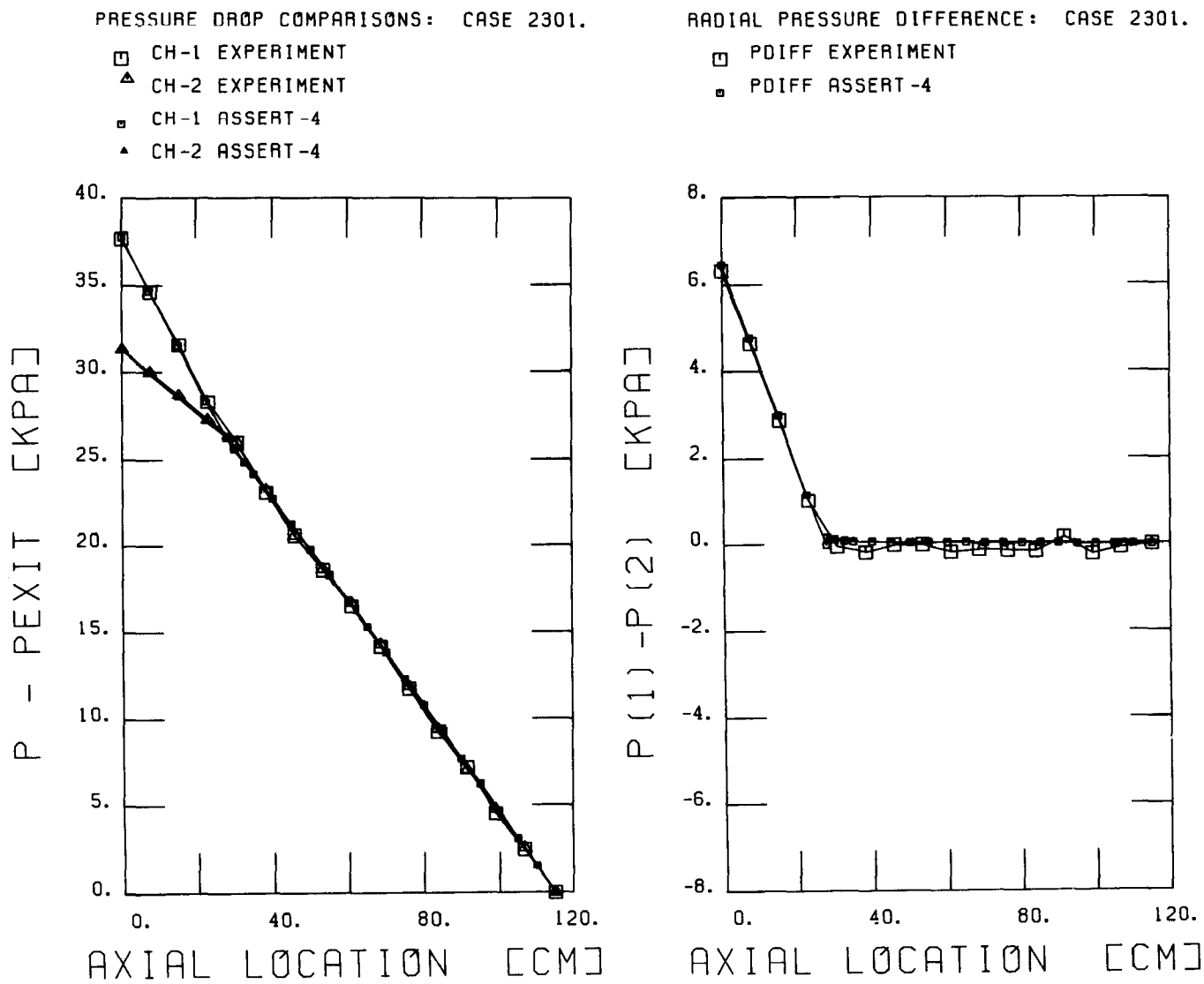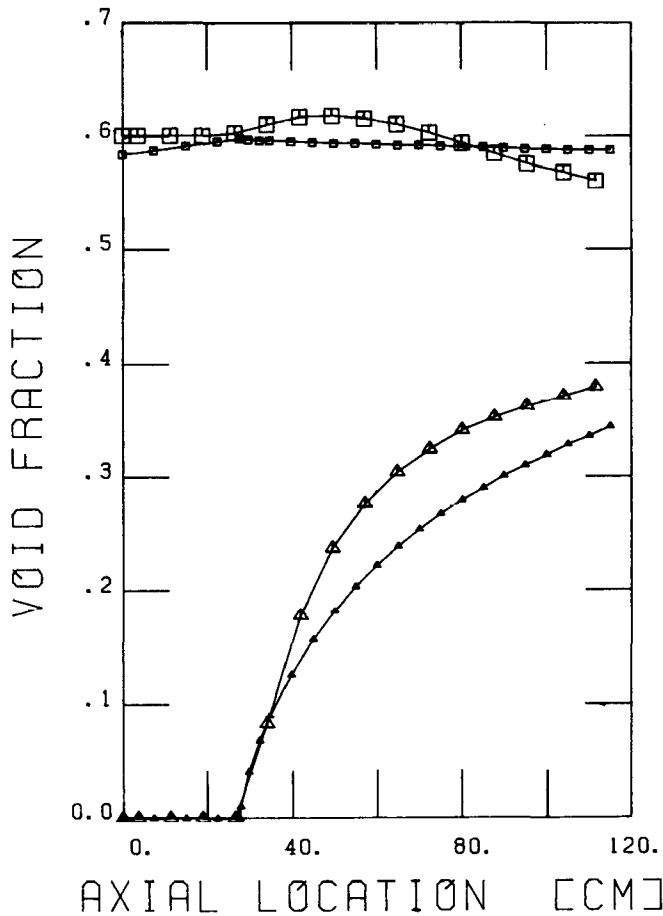

Figure 3: Typical experimental and computed pressure profile for vertical case V1.

VOID FRACTION COMPARISONS: CASE 2301.

□ CH-1 EXPERIMENT
△ CH-2 EXPERIMENT
▫ CH-1 ASSERT-4
▲ CH-2 ASSERT-4

LIQUID FLOW RATE COMPARISONS: CASE 2301.

□ CH-1 EXPERIMENT
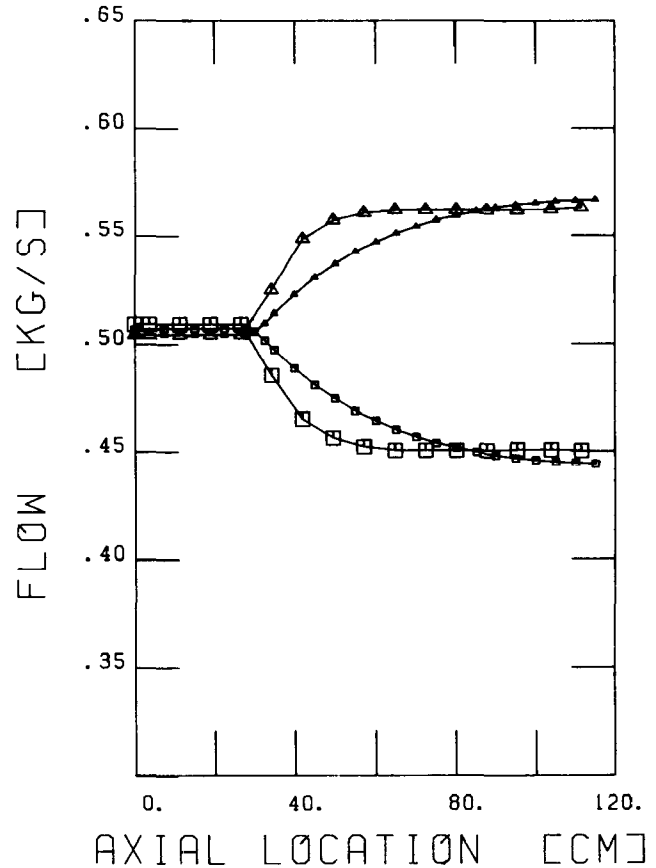△ CH-2 EXPERIMENT
▫ CH-1 ASSERT-4
▲ CH-2 ASSERT-4

Figure 4: Computed and measured profiles of void fraction and mass flux for vertical case V1 (square).

channels along the interconnection – were measured at several axial locations.

Until recently, code comparisons with these experiments had concentrated on modelling void fraction in particular cases [3], and on exhibiting correct qualitative trends. A sufficiently general model, however, should be able to reproduce trends quantitatively throughout the entire spectrum of experimental conditions. This is not an unrealistic demand in this case, as the data base and range of parameters are quite limited. The current research has modelled both void fraction and mass flux for the entire range of 17 experiments.

In the vertical orientation, only two mechanisms are active, the diversion cross-flow and the turbulent exchange. The experiments are well documented and good agreement with measured pressure drops was first obtained by a single-phase friction factor and Armand two-phase multiplier. Together with a good estimate of form loss, these closely determine the pres-

sure-driven diversion cross-flow. Pressure-driven cross-flow induces a co-current flow of air and water to flow from the higher pressure channel. In the experiments, pressure is quickly equalized in the slot, but the high void channel requires a higher initial pressure to overcome the two-phase pressure drop. A typical pressure profile is shown in Figure 3, along with computed pressures. The initial tendency in the vertical experiments is therefore for the recipient or low void channel to gain air and water from the donor. However, when the void fraction in the donor is high, the tendency towards turbulent exchange increases. This results in some counter-current flow, in which some liquid returns from the recipient to the donor and is replaced by air. This tendency is readily simulated by the diffusion model. Increased diffusion augments the tendency towards counter-current exchange.

Typical results showing void fraction and mass flux profiles are given in Figure 4. Note that in the void
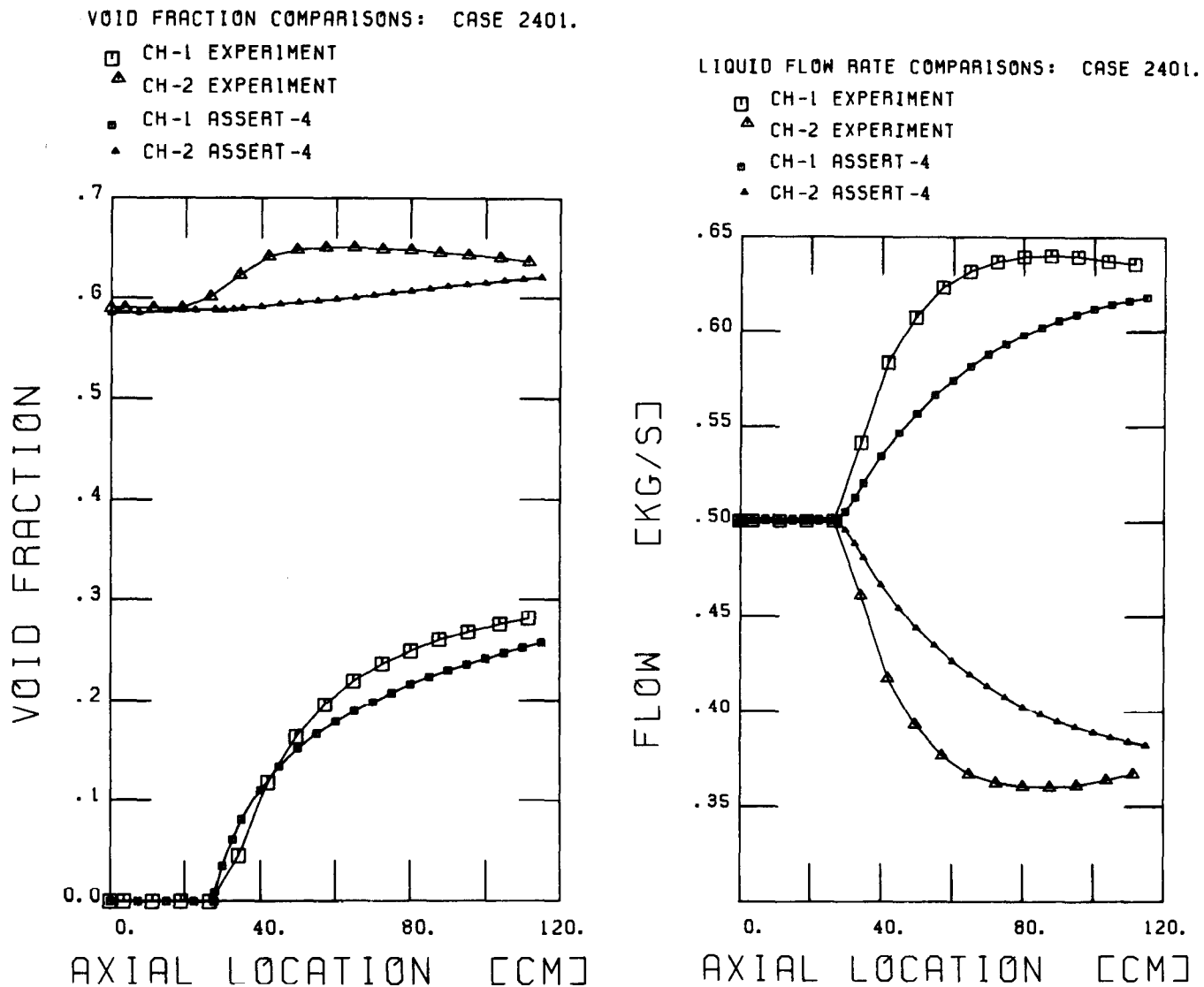
Figure 5: Computed and measured profiles of void fraction and mass flux for horizontal case $H_R^D - 1$ (square).

fraction profiles, donor void fraction initially increases somewhat, although air transfer is taking place to the receiver. This is typical of the experiments and is due to the fact that at the low experimental pressures (nominally 0.15 MN / m²) the air expands significantly as it descends the pressure gradient.

In the horizontal orientation, with one channel above the other, cross-flow is now driven by gravity as well as pressure and diffusion. In simulating the experiments, it was postulated that although the internal distributions would be different from the vertical case, the turbulent exchange would be of the same magnitude. Attention was therefore turned to the formulation of the relative velocity due to gravity.

Two orientations were examined in the experiments, with the donor or high void fraction channel above and below the recipient, denoted by H_R^D and H_D^R, respectively. In the former case, gravity drift does not cause exchange, and diversion cross-flow and turbu-

lent exchange dominate. In the latter, gravity drift is significant, but the initial interchange is a pressure-driven diversion cross-flow during which both air and water flow from the donor into the recipient above. Eventually gravity forces tend to become dominant, and counter-current lateral flow is set up.

Figures 5 and 6 show typical comparisons for the horizontal case $H_R^D - 1$ and its inverse $H_D^R - 1$. This particular pair of experiments was chosen because of the interesting behaviour of mass flux. This clearly illustrates that the initial tendency towards pressure-driven co-current exchange is eventually overcome by gravity-driven counter-current exchange. Further details of the comparisons are given in References 3 and 12.

Similar experiments have recently been completed by Tapucu [12] in which the channels were fabricated to a form that simulates the shape of neighbouring subchannels in a rod bundle, as shown in Figure 7. In

VOID FRACTION COMPARISONS: CASE 2411.

☐ CH-1 EXPERIMENT
△ CH-2 EXPERIMENT
■ CH-1 ASSERT-4
▲ CH-2 ASSERT-4

LIQUID FLOW RATE COMPARISONS: CASE 2411.

☐ CH-1 EXPERIMENT
△ CH-2 EXPERIMENT
■ CH-1 ASSERT-4
▲ CH-2 ASSERT-4

VOID FRACTION

AXIAL LOCATION   [CM]
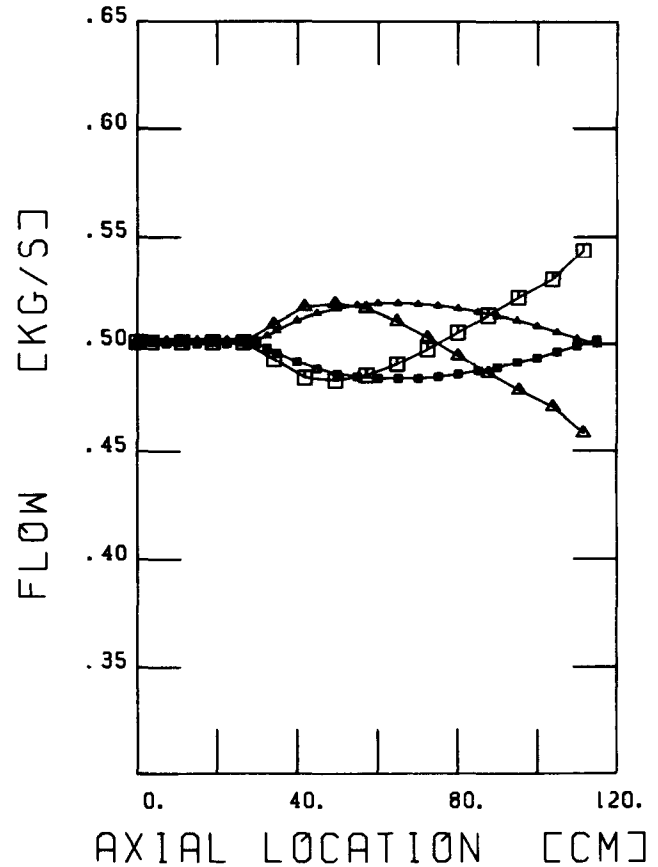
FLOW   [KG/S]

AXIAL LOCATION   [CM]
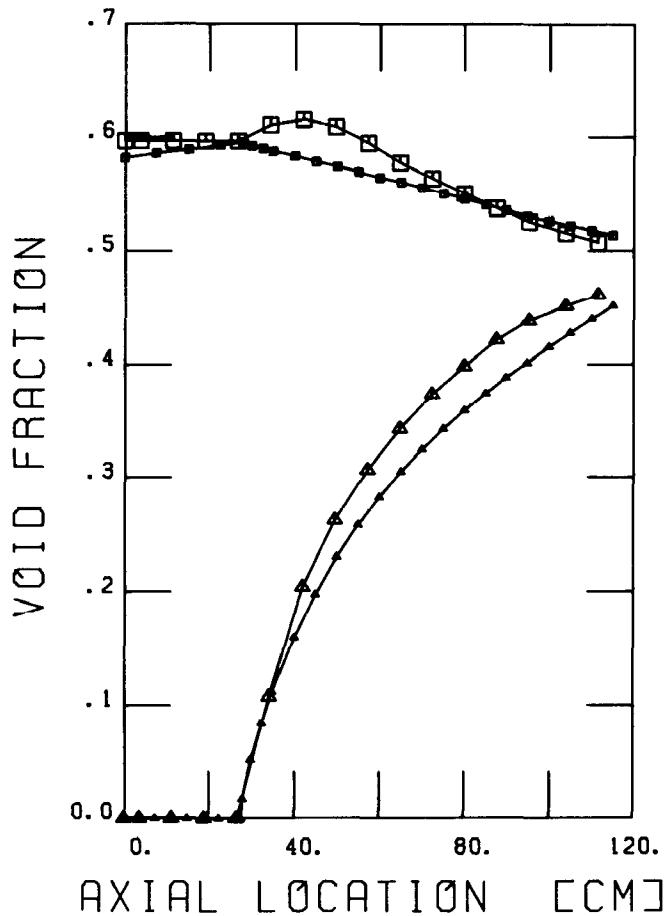
Figure 6: Computed and measured profiles of void fraction and mass flux for horizontal case $H_D^R - 1$ (square).

this case, the channels were run in five orientations, vertical and both horizontal in positions mentioned above, plus horizontal equal elevation and inclined orientations. All 24 of these experiments were simulated using ASSERT, but only representative cases are shown here.

Computed and experimental results are shown for two reciprocal cases in Figures 8 and 9. Again, the cross-over tendency is apparent in the mass flux profile and is simulated quite well by the program. Full details of the comparisons are given in Reference 12.
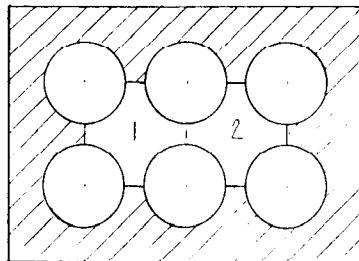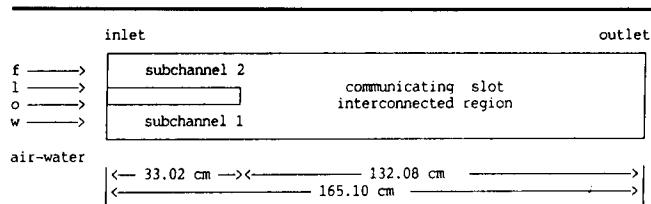
Comparison with Experiments in Vertical Bundles
The first bundle experiments used for validation were conducted by Bosio and Imset, using a vertical 7-rod bundle [14]. The bundle consisted of one electrically heated 3.6-m-long centre-rod, with a uniform axial power and six unheated peripheral rods (Figure 10). Simultaneous measurements of subchannel void frac-

tions were performed in the marked zones of Figure 10 by means of an impedance probe at three axial levels. The average void in the subchannels was calculated by integrating the local values. Measurements were obtained at the various mass fluxes around $1{,}500 \, \text{kg} \, \text{m}^{-2} \, \text{s}^{-2}$, 16 and 30 bars pressure, and about 5°C inlet subcooling.

Both ASSERT and COBRA-IV were used to simulate the complete repertoire of six experiments, without tuning to fit any particular experiment. ASSERT successfully simulates the experiments, and the difference between the ASSERT predictions and the experimental results averages less than 10% as typically shown in Figure 10. COBRA does not predict sufficient void migration into the unheated channel, as the COBRA mixing model is inadequate for two-phase flow. Further comparisons are discussed in Reference 4.

The experiments used in a second validation exercise were conducted by Nylund *et al*. Two bundles

159

```
              inlet                                              outlet
  f ———>        ┌──────────────────────────────────────────────┐
  l ———>        │  subchannel 2                                 │
  o ———>        │  ┌────────────────┐   communicating  slot     │
  w ———>        │  └────────────────┘   interconnected region   │
                │  subchannel 1                                  │
  air-water     └──────────────────────────────────────────────┘
                <— 33.02 cm —><———————— 132.08 cm ——————————>
                <————————————— 165.10 cm ——————————————>
```

- two rod-bundle subchannels on a square pitch
- adiabatic, air-water
- 7 vertical flow cases
- 17 horizontal flow cases

Experiment Geometry :

		Subchannel Data : (per subchannel)	
channel length	= 165.10 cm	flow area	= 1.1663 cm²
slot length	= 132.08 cm	hydraulic diameter	= 0.7620 cm
gap clearance	= 0.1660 cm	wetted perimeter	= 6.1223 cm
rod diameter	= 1.7580 cm	centroid distance	= 1.8660 cm

Figure 7: Geometry of the Tapucu experiment bundle-type subchannels.

were tested, one with 6 rods and one with 36 + 1 rods [15]. Both were uniformly heated with rods of 13.8 mm outer diameter and 4.4 m heated length. In the 36 + 1-bundle, an unheated centre rod of 20 mm diameter was used. The void was measured with a multi-beam gamma ray densitometer. By manipulating the beam in the radial direction it was possible to measure the void in different zones of the bundle. The 36 + 1 bundle was divided in three zones (rings) as shown in Figure 11. The measurements were taken at several axial locations in the bundles. Mass flux was again about 1,000 $kg\,m^{-2}\,s^{-1}$, pressure 50 bars; subcooling varied from 1° to 20°C.

For the 36 + 1-rod bundle, the scatter in the measurements of zones 1 and 2 was too large for meaningful comparison; the measurement in the remaining zones are quite consistent, as shown for zone 4 in Figure 11a. Comparisons were made only for bundle average, and zones 3 and 4 because of the lower scatter in the experimental results.

Typical ASSERT and COBRA-IV predictions for zone 4 are shown in Figure 11b, and are in good agreement with experimental results. In all of the cases, the COBRA or ASSERT predictions showed reasonable agreement. Comparisons for all the experiments are given in Reference 5.
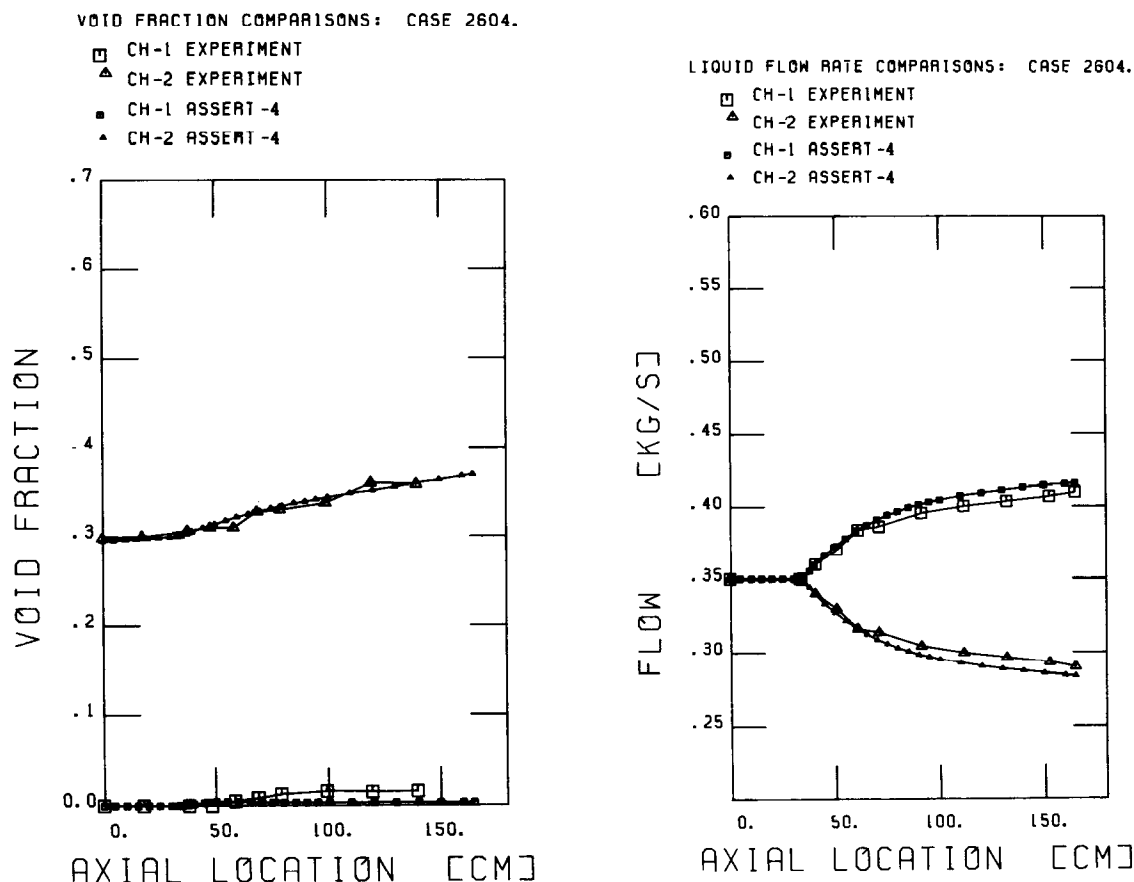

Figure 8: Computed and measured profiles of void fraction and mass flux for horizontal case H_R^D − 4 (bundle).
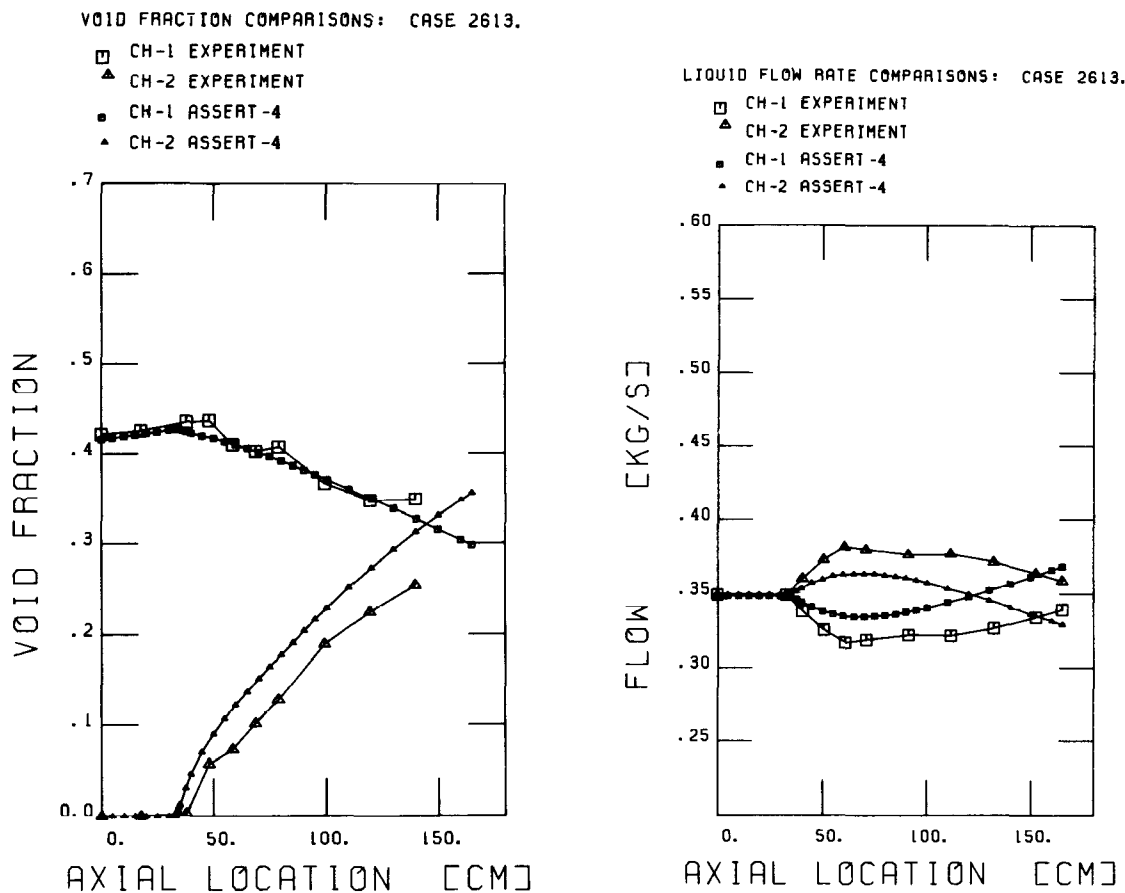
160

VOID FRACTION COMPARISONS: CASE 2613.

□ CH-1 EXPERIMENT
▲ CH-2 EXPERIMENT
■ CH-1 ASSERT-4
▲ CH-2 ASSERT-4

LIQUID FLOW RATE COMPARISONS: CASE 2613.

□ CH-1 EXPERIMENT
▲ CH-2 EXPERIMENT
■ CH-1 ASSERT-4
▲ CH-2 ASSERT-4

Figure 9: Computed and measured profiles of void fraction and mass flux for horizontal case $H_D^R - 3$ (bundle).

EXPERIMENTS OF BOSIO AND IMSET

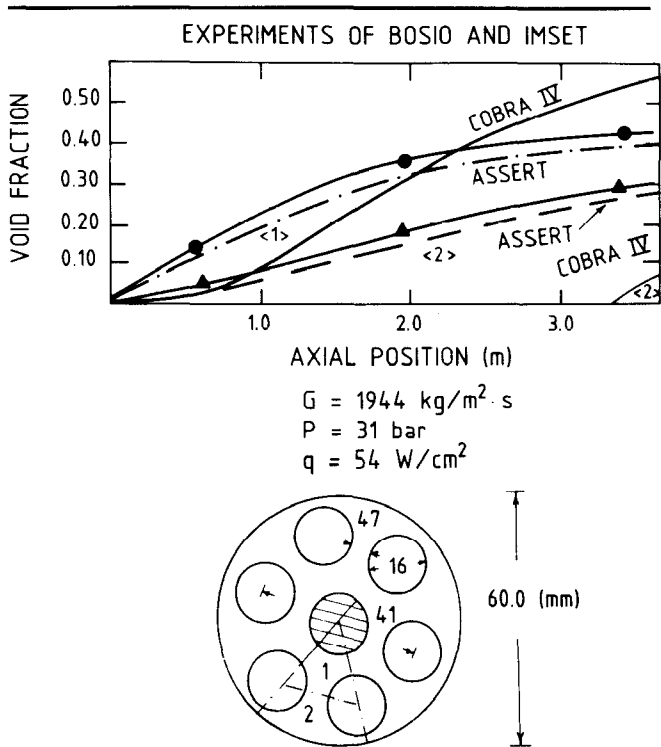G = 1944 kg/m² · s
P = 31 bar
q = 54 W/cm²

60.0 (mm)

Figure 10: Bosio and Imset experiments: geometry and a typical comparison of computed and measured void profiles.

Validation for CANDU 37 Rod Bundle Geometries

A series of experiments, sponsored by the Atomic Energy of Canada – Ontario Hydro CANDEV co-operative agreement, have been completed in the Chalk River Nuclear Laboratories U1 experimental facility to measure critical heat flux (CHF) in a full-size 6 m horizontal channel, containing an electrically heated simulated string of CANDU 37-rod fuel bundles [16]. The experiments used for the comparisons had a non-uniform exit-biased cosine axial heat flux profile. The bundles were tested in the CRNL-U1 loop, which supplied light water coolant at flows, temperatures, and pressures covering the range of interest to CANDU operation and subject to the following limits: pressure 13.9 MPa, power 12.25 MW, and flow 17.0 kg/s. Tests were completed at four nominal pressure levels, six nominal flows, and seven nominal values of inlet subcooling, and results included pressure, temperature, and conditions corresponding to the first detectable occurrence of CHF on the available instruments, as evidenced by a surface temperature rise of at least 2°C, associated with a small increment in electrical power to the bundle. Resistance temperature devices (RTD) and sliding thermocouples were used to measure rod temperatures.
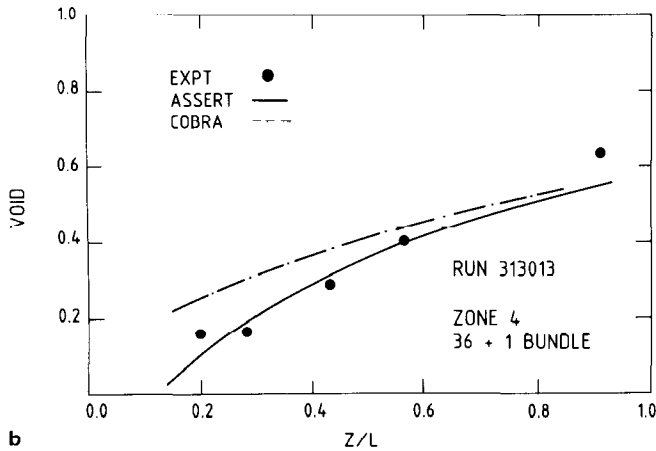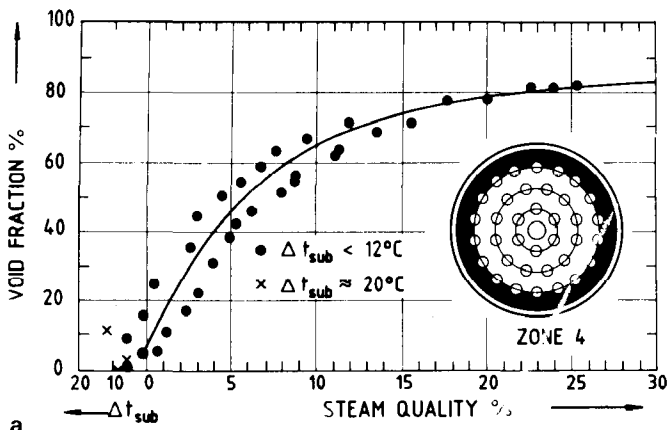
161

Figure 11: Marviken experiments: a) typical data, and b) typical comparison of computed and measured void profiles.
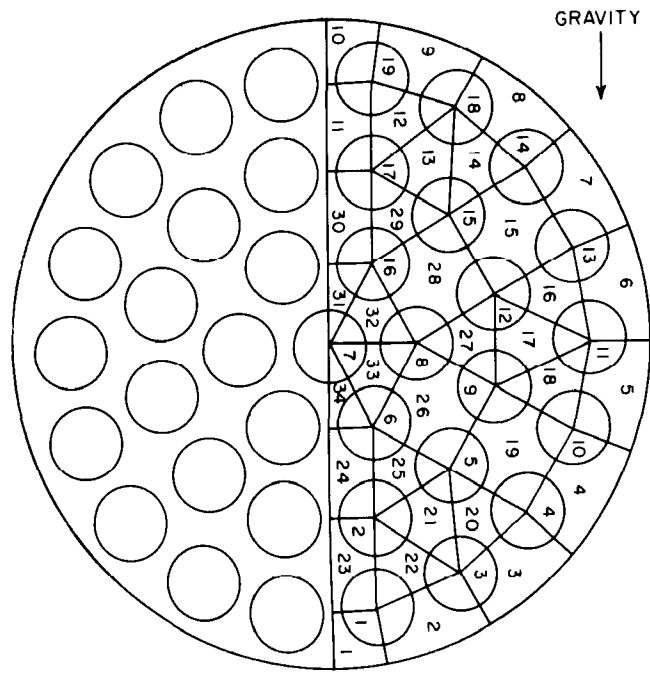

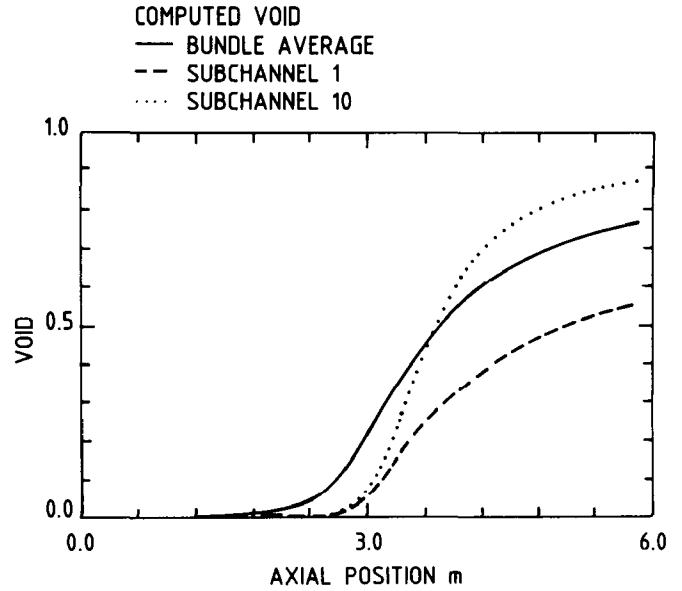Figure 12: Subchannel and rod numbering in ASSERT for a 37-rod bundle simulation.

Figure 13: Pressure drop and void profiles for a typical 37-rod experimental case.

Prediction of Flow Distribution

Symmetry is used to advantage in modelling the bundle in ASSERT, and rod and subchannel numbers are given in Figure 12. The axial layout included end-plates and spacer planes. The first task is to check that flow distribution is calculated adequately. Unfortunately, there are no detailed experimental data that can be used directly to check distribution. The overall pressure drop is one criterion that can be used, and, equally important, the overall pressure profile can be used to check single- and two-phase pressure drop calculations and the onset of local boiling.

Pressure profile predictions: A comparison of ASSERT and measured pressure profiles is given for a typical case in Figure 13; the pressure drop profile is in good agreement with the experimental measurements. The point of change in slope of the pressure drop profile from a linear to non-linear relationship with axial position, indicates the axial location of the onset of significant void in the bundle.

This additional validation of the ASSERT results is important, as the onset of void occurs significantly upstream of the point at which bulk boiling would be computed to commence on a cross-sectional average basis. In one-dimensional calculations, this effect is usually accounted for by incorporating a subcooled boiling correlation, but may, in fact, be primarily due to the onset of boiling in the hotter subchannels. The fact that ASSERT predicts the apparent location of this point suggests that calculation of flow distribution within the subchannels is adequate.

Figure 13 also shows predictions of bundle average void and the void in subchannels 1 and 10. Figure 12 shows that these are equivalent subchannels at the bottom and top of the bundle, respectively. The void in
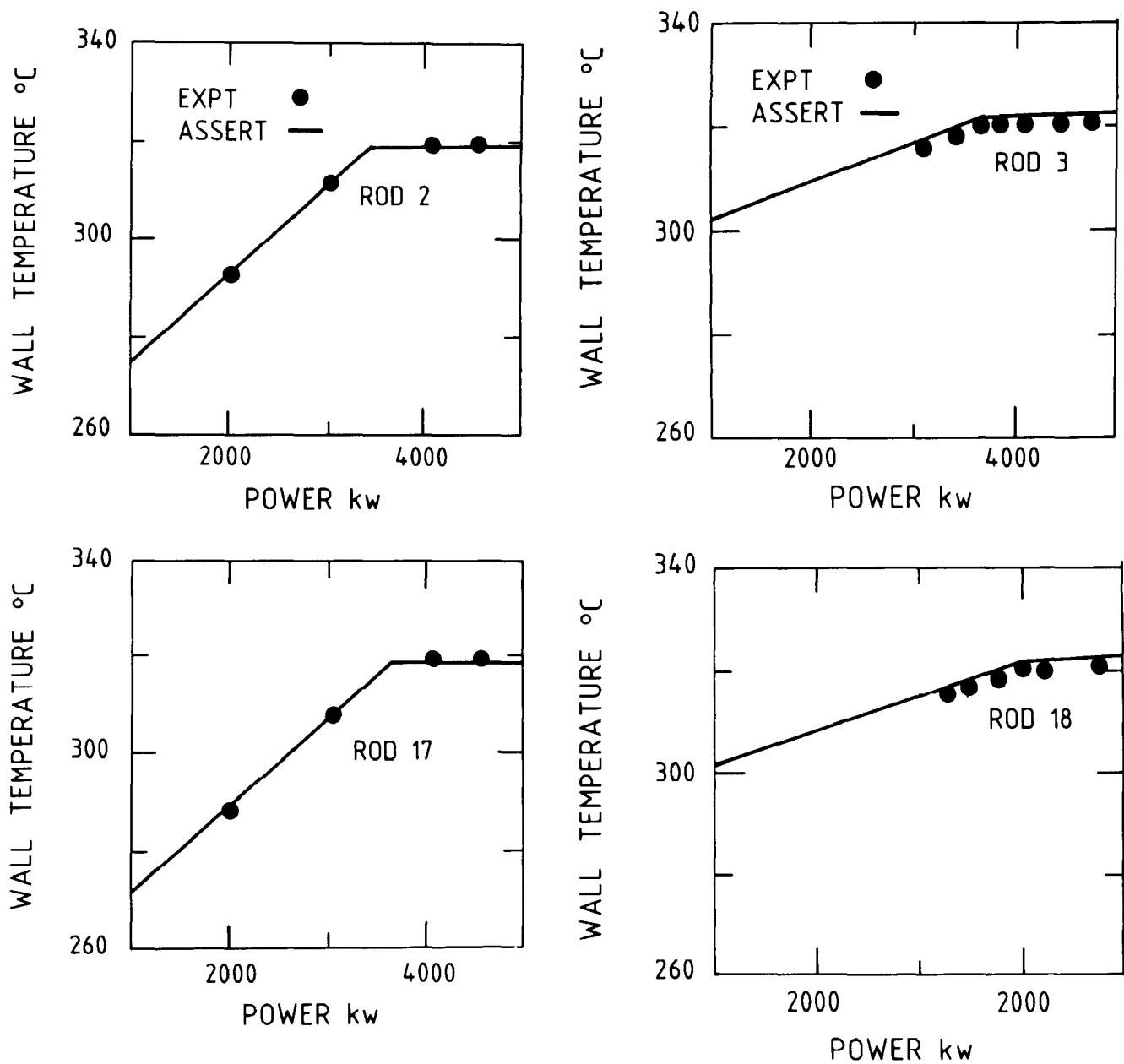
Figure 14: Measured and computed rod surface temperatures for a typical 37-rod case, showing two sets of upper and lower rods, for inner and outer subchannels.

the upper channel is predicted to be significantly higher in all cases. Comparisons with the experimental voids are not possible, as void was not measured.

Rod temperature predictions

A further means of checking the calculation of flow distribution is to calculate rod temperatures in ASSERT. This has been done for several representative experiments. The fuel model in ASSERT does not address electrical heaters, so the surface temperature of a rod section was calculated from the predicted fluid conditions in the subchannel facing the appropriate thermocouple, using boiling heat transfer correlations.

Comparisons between rod temperatures computed

by ASSERT and the thermocouple measurements are given for two representative situations in Figure 14. The onset of nucleate boiling is shown clearly by the change in slope of the temperature curve, and the predictions agree well with the experiment. Furthermore, two interesting observations can be made. For the subchannels inside the bundle, it appears that buoyancy effects in the liquid are significant, as the upper subchannel of any geometrically similar pair reaches incipient boiling ahead of the lower one, as shown in Figure 14. However, in the outer subchannels this buoyancy effect is overridden by the stronger effect of eccentricity. The lower outer subchannels are smaller in size than the upper ones; this makes the
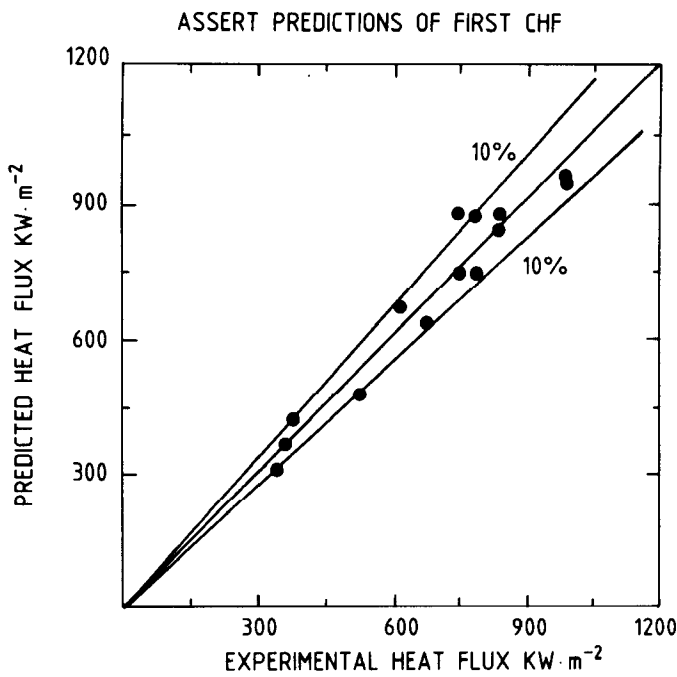
163

ASSERT PREDICTIONS OF FIRST CHF

(Figure: plot of PREDICTED HEAT FLUX KW·m^{-2} vs EXPERIMENTAL HEAT FLUX KW·m^{-2}, with axes at 300, 600, 900, 1200, 10% bands shown.)

Figure 15: Measured and computed CHF for a 37-rod typical experimental case.

Table 1: Nomenclature

Variable	Description
C_0	Phase distribution parameter
F	Wall friction
g	Acceleration due to gravity
h	Mixture enthalpy
h_g, h_f	Phasic enthalpy
j	Mixture volumetric flux, $(aV)^g + (\alpha V)^f$
P	Pressure
q	Heat transfer rate
t	Time
U	Mixture axial velocity
U_r	Relative axial velocity, $U_g - U_f$
V	Mixture velocity
V_r	Relative velocity, $V_g - V_f$
v_{gj}	Drift velocity lateral
V_r	Lateral relative velocity, $V_g - V_f$
$V\infty$	Bubble rise velocity
V_{gj}	Drift velocity
U_{gj}	Drift velocity axial
V_g, V_f	Phasic lateral velocity
α	Void fraction, $\alpha = \alpha_g$
α_0	Equilibrium void fraction
α_g, α_f	Phasic void fraction, $\alpha_g + \alpha_f = 1$
l	Centroid-to-centroid distance between subchannels
ϕ	Centroid-to-centroid angle
ρ	Mixture density
ρ_g, ρ_f	Phasic density
σ	Surface tension
ε	Diffusion parameter

Subscripts

if	Interface-to-liquid
ig	Interface-to-vapour
f	Liquid
g	Vapour
w	Wall
wf	Wall-to-liquid
wg	Wall-to-vapour

Superscripts

–	Average
→	Vector
′	Per unit length
″	Per unit area
‴	Per unit volume

volumetric heat input higher and causes them to boil first, also as shown in Figure 14. Further details are given in Reference 17. Clearly, the onset of nucleate boiling is influenced by single-phase turbulent mixing in the liquid. The single-phase mixing model of Rogers and Rosehart [18] is used in ASSERT.

Critical Heat Flux Predictions

Having established that ASSERT adequately reproduces the measured pressure and temperature profiles, the next task is to compare CHF predictions.

Because of the non-uniform heat flux distribution, CHF occurs upstream of the end of the bundle, and not at the exit as in the case of uniform heat flux distribution. In this comparison, the total power was increased until the code predicted CHF somewhere in the bundle. Since the predicted location of CHF in the bundle is not necessarily that observed in the experiment, the heat flux is further increased until the predicted CHF location is at the same axial position as that observed in the experiment. The values of heat flux that first gave rise to a computed CHF anywhere in the bundle are referred to as 'first CHF predictions.'

In assessing these comparisons, it is also important to realize that the experimental data are not absolute, but have an associated RMS error. As discussed in Reference 16, the experimental CHF RMS error is about 5% for a tube. CHF measurements in a bundle having a non-uniform axial heat flux profile are more complicated than those of the tube experiments, so an RMS error greater than 5% is probable. The first CHF predictions, using the Whalley model in ASSERT, are given in Figure 15 for 14 experimental cases chosen to cover the range of variables.

In all cases, ASSERT predicts CHF to occur first in the top rod, number 19, of the outer ring in the bundle, subchannel 10. This was also observed experimentally for low-flow cases, while for the rest of the cases, CHF occurs in the top rod, number 17, in the second ring. In all cases, ASSERT predicts CHF will occur in this second subchannel ring (subchannels 12 and 13) with a slight increase in power. As discussed previously, these computations represent a first application of ASSERT to CHF prediction, and it is clear that the results are reasonable.

More recent work with ASSERT has been directed towards improving the CHF methodology, and extending the ASSERT CHF repertoire, in particular to include the CHF table method [18]. These extensions are de-

scribed in Reference 19, and extensive comparisons have been made with CHF data for a number of different experiments in horizontal rod bundles. A detailed report on these comparisons is in press. Comparisons of ASSERT predictions to CHF experiments in a horizontal 28-rod bundle have been completed by Ontario Hydro [20].

Conclusions

The first phase of the ASSERT, advanced subchannel code development has been completed, illustrating that the code is capable of computing flow and phase distribution effects in horizontal channels and fuel bundles. In the U1 experiment, there were no direct measurements of flow distribution, so indirect indications of distribution were used for comparison. The code was able to match pressure profiles and rod temperatures quite closely. Finally, a first attempt at computing local CHF was made, and the results were encouraging.

Acknowledgements

References

1. Judd RA, Tahir A, Kiteley JC, Carver MB, Rowe DS, Stewart DG, Thibeault PR. ASSERT-4 (Version 1) User's Manual. Atomic Energy of Canada Limited, AECL-8573, 1984.

2. Stewart CW, Wheeler CL, Cena RJ, McMonagle CA, Cuta JM, Trent DS. COBRA-IV – The model and methods. Battelle Pacific Northwest Laboratories, BNWL-2214, July 1977.

3. Carver MB, Tahir A, Rowe DS, Tapucu A, Ahmad SY. Computational analysis of two-phase flow in horizontal bundles. Nucl Eng and Design 1984.

4. Tahir A, Carver MB. ASSERT and COBRA predictions of flow distribution in vertical bundles. CNS / ANS Conference on Numerical Methods in Nuclear Engineering, Montreal, 1983.

5. Tahir A, Carver MB. Comparisons of ASSERT subchannel code with Marviken bundle data. 10th Simulation Symposium on Reactor Dynamics and Plant Control, St. John, New Brunswick, April 9–10 1984.

6. Zuber N, Findlay JA. Average volumetric concentrations in two-phase flow systems. J Heat Transfer 1965; V (87).

7. Lahey RT. Two-phase flow boiling in nuclear reactor. NEDO-13388, General Electric Co., 1974.

8. Rudzinski KF. Two-phase turbulent mixing for air-water flows. MASc Thesis, University of Windsor, 1970.

9. Ohkawa K, Lahey RT. The analysis of CCFL using drift flux model. Nuclear Engineering and Design 1980; V (61).

10. Whalley PB et al. Calculations of CHF using an annular flow model. 6th Int Heat Transfer Conference, Toronto, 1978.

11. Tapucu A, Gencay S. Experimental investigation of mass exchange between two laterally interconnected two-phase flows. Ecole Polytechnique report CDT P-533, Montreal, 1980.

12. Kiteley JC. Numerical modelling of phase distribution in interconnecting subchannels. 5th Inf Conference on Numerical Methods in Thermal Problems, Montreal, 1987.

13. Tapucu A, Geckinli M, Troche N. Experimental investigation of mass exchange between two laterally connected two-phase flows. Subchannel geometry. Reports IGN-556 and 557, Ecole Polytechnique du Montreal, 1984.

14. Bosio J, Imset OR. Experimental two-phase flow investigating in a 7-rod bundle. Inst Atomenergi report SD-136 / SDS-70, 1970.

15. Nylund O et al. Hydrodynamic and heat transfer measurements on a 36-rod Marviken fuel element. Frigg-2-R4-477 / RTL-1007, 1968; and Frigg-1-R-4-422 / RTL-914, 1967.

16. Tahir A, Stewart DG. Prediction of critical heat fluxes in fuel bundles via the ASSERT subchannel codes. XII Simulation Conference on Reactor Dynamics and Control, McMaster University, 1986.

17. Tahir A, Bernard C. Comparison of rod surface temperature of a 37-rod bundle against measurements under forced convection and nucleate boiling. XI CNS Simulation Symposium on Reactor Dynamics and Control, U of New Brunswick, 1985.

18. Rogers JT, Rosehart RG. Mixing by turbulent interchange in fuel bundles correlations and inferences. ASME Paper 72-HT-53, 1972.

19. Groeneveld DC, Cheng SC, Doan T. The CHF look-up table, a simple and accurate method for predicting critical heat flux. Heat Transfer Engineering 1986; 7 (1–2).

20. Szymanski JK, Midvidy WI. Comparison of CHF predictions by ASSERT-IV with measurements in 28-element fuel. CNS Second International Conference on Simulation Methods in Nuclear Engineering, Montreal, 1986.